Case study on the influence of electrostatic charges on particle concentration in turbulent duct flows

H. Grosshans[a,*], L. Villafañe[b], A. Banko[b], M.V. Papalexandris[c]

[a] *Physikalisch-Technische Bundesanstalt (PTB), Bundesallee 100, 38116 Braunschweig, Germany*
[b] *Department of Mechanical Engineering, Stanford University, CA*
[c] *Institute of Mechanics, Materials and Civil Engineering, Université catholique de Louvain, 1348 Louvain-la-Neuve, Belgium*

Abstract

Preferential concentration of inertial particles in wall-bounded turbulent flows is of paramount importance and, thus, subject of fundamental research. In practical applications of confined particle-laden flows the particles experience frequent collisions with the piping system which may result in an unwanted electric charge separation through triboelectric effects. The consequential occurrence of electrostatic forces alters the particle trajectories and their distribution. In this work the influence of charges on the averaged concentration of inertial particles in a fully developed turbulent duct flow was investigated by means of a combined numerical and experimental approach. The order of magnitude of the potential charge accumulation was estimated and imposed in a parametric study to the particulate phase in the simulations. Also, a new numerical approach based on the stochastic parcel method is introduced that allows to handle a large number of charged particles in a Lagrangian framework. This new approach extends standard formulations by including the effect of electrostatic forces on each parcel. The simulations demonstrate that the concentration profiles are for the most part independent of the prescribed charge except in the region close to the walls. The peaks of the particle number density at the walls caused by turbophoresis are strongly reduced through the local increase of repelling electrostatic forces. The comparison of numerical with experimental data indicates that the particles in the experimental setup could be affected by a surface charge density of the order of 100 $\mu C/m^2$. The presented results aim to elucidate the impact of electrostatic forces in the particle distribution in wall-bounded particle-laden flows.

Keywords: electrostatics, particle concentration, duct flows, experiment, simulation

1. Introduction

Preferential concentration of inertial particles in fully-developed wall-bounded turbulent flows is of relevance to many industrial applications, such as pneumatic powder conveying (Grossel, 2012), pulverized coal combustion (Kuerten et al., 2011) or particle-based solar receivers (Lenert and Wang, 2012). For this reason, this type of flows is subject to experimental research since decades. Noteworthy classical works include those by Tsuji and Morikawa (1982) and Tsuji et al. (1984) who collected a large set of data concerning the mean velocity of powders in vertical and horizontal flows through circular pipes. This kind of experimental study requires the usage of a long feed-line in order to obtain a fully-developed flow at the test section and to ensure that the particles are independent of their initial conditions. However, as the particles are advected along the piping system they may experience frequent collisions with the walls and between each other. If the powder and the piping system are of a different kind of material their contact results in an electric charge separation through triboelectric effects (Soo, 1971). Under those circumstances a considerable amount of electric charge might be accumulated on the surface of the particles or on the structural components of the facility.

One easily observable consequence is the deposition of particles on the surfaces of the test section (Adhiwidjaja et al., 2000; Guardiola et al., 1996; Schwindt et al., 2017). If no adequate measure is taken, such as the usage of an antistatic agent (as done by Tsuji and Morikawa (1982); Tsuji et al. (1984)), particle deposition might alter near-wall particle concentrations. Also, deposition layers may induce detrimental effects on the experiments, i.e., constrain optical access and

*Corresponding author
Email address: holger.grosshans@ptb.de (H. Grosshans)

light transmission. Another, less obvious, implication of electrostatic forces is the modulation of the particle trajectories of airborne particles. In an experimental setting, the exact influence of electrostatics on the measured particle concentration statistics is unknown. While electrostatic forces may contribute to particle deposition, the formation of deposits is also affected by van der Waals forces and other adhesive forces dependent on surface properties and on the presence of liquid films. In an industrial context, the formation of deposits has the potential to impair the performance of the facilities by reducing the effective cross-sectional area of pipes or other devices (Hendrickson, 2006; Song and Mehrani, 2017; Sippola et al., 2018). Also, excessive local charge accumulation can effectuate sparks which challenges the operational safety of a plant (Glor, 2003; Fath et al., 2013; Egan, 2017).

Experimental measurements in the near-wall region in particle-laden flows are challenging due to the wall interference with optical measurement techniques, and also because of the temporal and spatial resolution required to capture the small scales of the particle and flow structures of interest. Limited data is available of gas and particle phase statistics near walls (Eaton and Fessler, 1994), and measurements are often restricted to relatively large flow scales and particles with diameters larger than the dominant near-wall eddies (Sumer and Deigaard, 1981). Conversely, numerical simulations have been extensively used to study near-wall phenomena. A remarkable early contribution was the ability of capturing the accumulation of particles in the viscous sublayer through *turbophoresis*, i.e. the tendency of particles to migrate in the direction of decreasing turbulent intensity, by means of direct numerical simulations (DNS) (Kallio and Reeks, 1989; McLaughlin, 1989). More recent examples include the explanation of the mechanisms for particle transfer in the turbulent boundary layer by Marchioli and Soldati (2002) and the computation of the inertial migration of particles in laminar square duct flow by Tabaei Kazerooni et al. (2017). Nonetheless, simulations rarely consider the possible effect of arising electrostatic forces which are expected in real particle-laden flows.

Previous numerical works proposing approaches to predict the charge build-up process of solid-fluid mixtures incorporated different levels of simplifications. For example, the simulations by Hogue et al. (2008) described the charging of particles but neglected the influence of aerodynamic forces on their trajectories. Watano et al. (2003) included drag forces in the numerical framework but they assumed the gaseous phase to follow a predefined velocity profile, i.e. the interaction between particle dynamics and turbulence was not accounted for. The same counts for the studies of Kolniak and Kuczynski (1989) and Tanoue et al. (1999, 2001) who solved the Reynolds-Averaged Navier-Stokes equations for the turbulent gas flow. The fluid-particle interaction was computed through large-eddy simulations (LES) by Lim et al. (2012). Lim et al. (2012) used large-eddy simulations (LES) to compute fluid-particle interaction but their focus was directed to the influence of an external electric field on already charged particles. The authors of the present paper implemented dynamic models to predict the contact charging of particles when colliding with a solid surface or with each other into a computational fluid dynamics solver. Employing this computational framework, generic geometries such as channel and pipe flows were studied while accounting by DNS (Grosshans and Papalexandris, 2017a) or LES (Grosshans and Papalexandris, 2016b) for the turbulence of the carrier fluid. Albeit electrical forces were included in the set of equations, the size of the flow-through vessels was small, and the aim was to study the initial charge build-up. The accumulated charge was rather low and did not significantly influence particle dynamics. All the above mentioned studies employ a Lagrangian framework to track the particle trajectories. Due to the computational cost of particle-particle interactions this choice limits the amount of particles and, thus, the size of the computational domain to be considered. With this in mind, Kolehmainen et al. (2018) and Ray et al. (2018) developed Eulerian approaches to treat charging particle-laden flows which comes on the expense of loosing the particles' time-history.

To sum up, the influence of accumulated electrostatic charge on the preferential concentration of particles in wall-bounded flows in large-scale facilities is not known to date. While experimental results may be affected by triboelectric charging, quantification of its precise impact is at present lacking. In order to evaluate its contribution we investigated the influence of electrostatic forces on inertial particles for a test case by comparison of numerical and experimental results. The considered test case regards a fully-developed particle-laden flow through a vertical duct with a square cross-section. In the simulations, a constant surface charge density was initially assigned to the particles. The process of the build-up of charge was examined in previous studies by the authors (Grosshans and Papalexandris, 2016b, 2017a). In total six simulations were performed where the value of the surface charge density was varied parametrically. LES were used to simulate the turbulent flow and both back reaction by the particles on the flow and particle-particle and particle-wall collisions were accounted for.

This paper is organized as follows. The numerical methodology is outlined in section 2. In particular, a new numerical approach based on the stochastic parcel method is introduced that allows to handle a large number of charged particles in a Lagrangian framework. Section 3 presents the specific case that was experimentally and computationally studied. Results are discussed in the fourth section followed by the main conclusions.

2. Mathematical model and numerical methods

This section summarizes the in-house CFD solver employed in the present study. The solver utilizes a four-way coupled approach where the continuous gaseous phase is described in an Eulerian and the dispersed particulate phase in a Lagrangian framework (Elgobashi, 1994). The gaseous phase model, described by Grosshans and Papalexandris (2016b, 2017a), considers a dilute particle loading such that the volume fraction of the gaseous phase can assumed to be unity. The mass and momentum balance laws are given by the Navier-Stokes equations with constant diffusivities, namely

$$\nabla \cdot \boldsymbol{u} = 0 \tag{1a}$$

$$\frac{\partial \boldsymbol{u}}{\partial t} + (\boldsymbol{u} \cdot \nabla)\boldsymbol{u} = -\frac{1}{\rho}\nabla p + \nu \nabla^2 \boldsymbol{u} + \boldsymbol{F}_\mathrm{s} + \boldsymbol{F}_\mathrm{f}\,. \tag{1b}$$

In the above equations $\boldsymbol{u}$ denotes the gas velocity, p its pressure, ρ its density and ν its kinematic viscosity. A source term, $\boldsymbol{F}_\mathrm{s}$, accounting for the momentum transfer from the particulate to the gaseous phase is also introduced. The flow is forced in positive x-direction by adding a constant pressure gradient, $\boldsymbol{F}_\mathrm{f}$.

The governing equations of LES are obtained by applying a spatial filter operator to equations (1a) and (1b). Thus, the large-scale turbulent motions are directly resolved on the computational grid. On the other hand, the small sub-filter scales, which exhibit universal characteristics, are considered through an appropriate turbulence model. To this end, the implicit model by Boris et al. (1992) is applied. The above Eulerian equations are discretized by the Finite Difference Method (FDM). In particular, the convective terms are approximated by an up to fifth-order Weighted Essentially Non Oscillatory (WENO) scheme (Jang and Shu, 1996). The diffusive and pressure terms are approximated by fourth-order central differences and the time derivatives by an implicit second-order backward scheme. For further details concerning the numerical implementation the reader is referred to Gullbrand et al. (2001).

The particulate phase is treated according the numerical methodology proposed by Grosshans and Papalexandris (2017c) and implemented by Grosshans (2018). This methodology is extended to facilitate the treatment of a large amount of particles as outlined in the following. The novelty of the presented formulation lies in the inclusion of electrostatic forces in the stochastic formulation as outlined below.

In the current setting, the particle number density function is given by

$$Y = Y(\boldsymbol{u}_\mathrm{p}, r_\mathrm{p}, Q_\mathrm{p}; \boldsymbol{x}, t)\,. \tag{2}$$

This expression gives the probable number density of particles having a velocity of $\boldsymbol{u}_\mathrm{p}$, a radius of r_p and carrying an electrical charge of Q_p at a certain location, $\boldsymbol{x}$, and time instance t. In order to handle the large amount of particles the stochastic parcel method (Bracco, 1985) is adopted to approximate Y. Accordingly, the above function is discretized and subsequently integrated over the independent variables to obtain a set of computational parcels. Then, each parcel represents a finite number of particles (here: $\zeta = 10$ particles) and each parcel is tracked in a Lagrangian framework.

The trajectory of a parcel is altered by accelerations due to aerodynamic, $\boldsymbol{f}_\mathrm{ad}$, collisional, $\boldsymbol{f}_\mathrm{coll}$, gravitational, $\boldsymbol{f}_\mathrm{g}$, and electric field, $\boldsymbol{f}_\mathrm{el}$ forces. Particles of small size as those considered in the present study are additionally subjected to van der Waals forces, relevant for example during the formation of deposits and particle agglomerates. However, the influence of van de Waals forces on the trajectories of dilute airborne particles is small compared to that of electrostatic forces and thus, they are neglected herein.

For the aerodynamic acceleration, the particle drag coefficient is derived as a function of the particle Reynolds number following the classical correlation of Schiller and Naumann (1933). Furthermore, gravity accelerates the particles towards the positive x-direction.

Binary particle collisions and elastic reflection of the particles at the walls is accounted for. To enhance computational efficiency, a statistical technique that yields a collision frequency is employed (Stiesch, 2003). More specifically, it is assumed that the probability P_n that the particles of parcel n collide with the particles of parcel m during the time increment $\mathrm{d}t$ follows a Poisson distribution, namely

$$P_n = 1 - \mathrm{e}^{-\omega_{nm}\,\mathrm{d}t}\,. \tag{3}$$

In this equation, the time-averaged collision frequency ω_{nm} is defined as

$$\omega_{nm} = \pi \frac{\zeta_m \left(r_{\mathrm{p},n} + r_{\mathrm{p},m}\right)^2 |\boldsymbol{u}_{\mathrm{p,n}} - \boldsymbol{u}_{\mathrm{p,m}}|}{(\boldsymbol{e}_x \cdot \boldsymbol{\delta})(\boldsymbol{e}_y \cdot \boldsymbol{\delta})(\boldsymbol{e}_z \cdot \boldsymbol{\delta})} \tag{4}$$

where $\boldsymbol{\delta}$ is a vector pointing from the location of one parcel to the other, $\boldsymbol{e}_x$, $\boldsymbol{e}_y$ and $\boldsymbol{e}_z$ denote the unit vectors of the Cartesian coordinate system and $\cdot$ the scalar product. Numerically, a random number X is generated in the interval $(0, 1)$. If $X < P_n$, then no collision takes place whereas if $X \geq P_n$, then collision occurs. In order not to increase the number of computational parcels, the post-collision velocities of all particles associated with a parcel are assumed to be the same.

The specific force acting on a particle due to the electric field is calculated as

$$\boldsymbol{f}_{\mathrm{el}} = \frac{Q_{\mathrm{p}} \boldsymbol{E}}{m_{\mathrm{p}}} \tag{5}$$

where m_{p} is the mass of the particle. It is noted that the process of charge build-up is not considered in the present study, i.e. a charge Q_{p} is initially assigned to each particle (see section 3.3) which is then constant in time.

Concerning the computation of the electric field strength, $\boldsymbol{E}$, there are two different approaches available, namely Gauss' and Coulomb's law. Whereas Gauss' and Coulomb's law are mathematically equivalent, the numerical methods for solving them when dealing with a large number of particles may differ considerably in terms of accuracy and computational costs. For the proof of their equivalence and a detailed discussion concerning the advantages and disadvantages of each approach, the reader is referred to Grosshans and Papalexandris (2017c).

In the present study, a computational efficient and accurate hybrid scheme which combines both approaches which was proposed by Grosshans and Papalexandris (2017c) is applied. Therein, the interaction of an individual parcel with the space charge, i.e. with the electric field originating from the particle cloud, is calculated by Gauss' law. Furthermore, the derivation of the forces between parcels located close to each other (here: present in the same grid cell) is based on Coulomb's law.

According to Gauss' law, the divergence of the electric field is related to the volumetric electric charge density, ρ_{el}, by

$$\nabla \cdot \boldsymbol{E} = \frac{\rho_{\mathrm{el}}}{\varepsilon} \,. \tag{6}$$

In the above equation $\varepsilon = 8.854$ F/m denotes the electrical permittivity of the vacuum. In the context of the stochastic parcel method, ρ_{el} is defined as

$$\int_{\mathcal{V}} \rho_{\mathrm{el}} \, \mathrm{d}\mathcal{V} \;=\; \sum_{m=1}^{N} \zeta_m \, Q_{\mathrm{p},m} \,, \tag{7}$$

where $\mathcal{V}$ is a control volume containing N parcels.

For the case of charged particles, alternatively Coulomb's law can be used which reads for stochastic parcels

$$\boldsymbol{E}(\boldsymbol{r}) = \frac{\zeta_m \, Q_{\mathrm{p},m} \, \boldsymbol{r}}{4 \, \pi \, \varepsilon \, |\boldsymbol{r}|^3} \,. \tag{8}$$

Therein, $\boldsymbol{E}(\boldsymbol{r})$ is the electric field a particle is subjected to due to the presence of another parcel at a distance of $\boldsymbol{r}$ consisting of ζ_m particles carrying the charge $Q_{\mathrm{p},m}$. The influence of particles within the same parcel on each other, due to collisions or hydrodynamic forces, are not resolved in the stochastic parcel method. This fact also holds for the electrostatic forces in the formulation given above.

3. Case study

A fully developed particle-laden turbulent flow in a square cross-section duct was used as case study. The average particle concentration distribution computed for various levels of charge density was compared to experimental data for which the charge is unknown. Therefore, the aim of this study is to assess the sensitivity of particle motion to accumulated charge computationally. The flow conditions, particle properties and mass loading ratio are the same in simulations and experiments.

3.1. Description of experiments

The experimental data consist of profiles of averaged particle concentration from a particle-laden square duct facility at Stanford University. Ambient pressure and temperature air is fed to a blower that provides a constant flow rate during the experiments. The air is laden with particles via a volumetric feeder prior to entering a 5.4 m long vertical aluminum duct with a $H = 40$ mm wide square cross section. The development duct is followed by a 475 mm long borosilicate glass test section with a nominal internal cross-section of 40 mm × 40 mm, 2 mm thick walls, and 2 mm internal corner radii which is depicted in figure 1. The wind tunnel discharges to ambient conditions after the particles are collected in a cyclone separator. Further details of the experiments are given in Villafañe et al. (2017). The operational conditions of relevance for the present study are a Reynolds number based on the bulk velocity and test section width of $Re = 10\,000 \pm 0.7\%$, and ratio of mass loading of particles to air of 0.01. The particles used are made of nickel, with a density of $\rho_\mathrm{p} = 8900$ kg/m^3, and have a number-based mean diameter of 11.8 ± 0.5 µm. The particle-size probability distribution, as measured by a Coulter Counter, exhibits low probability tails that cover the range 6 µm to 20 µm. The distribution is shown in figure 2. The average Stokes number based on the mean particle diameter and the duct averaged Kolmogorov time scale is $St_\eta = 5$.

Particle concentration measurements were performed using planar optical techniques. The beam from a pulsed NdYag laser was expanded into a laser sheet that crossed the test section with constant thickness and width. The $1/e^2$ Gaussian beam thickness was 1.6 mm, and the sheet width was 25 mm. The laser sheet was aligned with the streamwise direction and inclined 18 degrees with respect to the wall normal, as shown in figure 1. This set-up configuration was needed to measure particle concentrations near the wall due to the curved test section corners. A high resolution CCD camera synchronized with the laser and perpendicular to the illumination sheet, acquired instantaneous and uncorrelated snapshots of the particles. Image processing algorithms were used to identify individual particles in each of the 2000 snapshots and to extract the coordinates of particle centroids that were used to compute concentration profiles.

3.2. Numerical set-up

The computations in the current study were performed using a computational domain that replicates the experimental square test-section duct and extends 15 times the duct width, H, in streamwise direction. Periodic boundary conditions were used in streamwise direction in order to mimic an infinite duct length, and no-slip is assumed for the gaseous phase at the sidewalls. Consistent with the experiments, a flow Reynolds number of $Re = 10\,000$ was imposed.

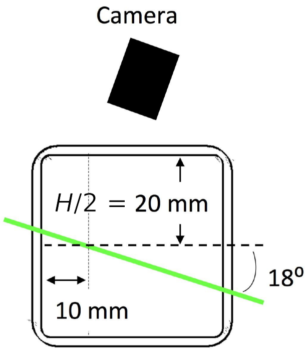

Figure 1: Laser sheet configurations used for measurements of mean particle concentration (Villafañe et al., 2017).

The duct was assumed to be of a conductive material and grounded This choice implies that an electrical charge which might be brought to the duct's surface upon contact with a particle, vanishes almost instantly towards ground. Nonetheless, particles residing in the vicinity of the walls are subject to forces by image charges. Thus, the duct walls constitute an equipotential surface which mathematically corresponds to setting the tangential component of $\boldsymbol{E}$ at the walls to zero when solving equation (6) (Moore, 1973). This boundary condition replicates the experimental development duct.

The results presented in the following are given in terms of the non-dimensional wall distance $y^+ = yu_\tau/\nu$ and time $t^+ = tu_\tau/H$ where u_τ is the friction velocity. Whereas we previously employed a coarse grid to provide qualitatively reliable results (Grosshans et al., 2018), the current simulations aim to resolve the viscous sublayer. Thus, the grid was refined in the vicinity of the wall where the first point was placed at $y^+ = 0.75$ and the grid spacing in the central region was $\Delta y^+ = 6$. In total, the mesh consisted of 6 million cells which were distributed on a parallel cluster and solved using Message Passing Interface (MPI).

The above described Eulerian-Lagrangian solver has been applied previously to simulate a wide range of dispersed flows such as LES and DNS of pneumatic powder conveying (Grosshans and Papalexandris, 2016b,a,c, 2017b; Schwindt et al., 2017; Grosshans and Papalexandris, 2017a). The mentioned references include a large amount of validation studies of various aspects of the solver, realized e.g. through grid resolution studies and comparison with experiments. In particular, the implementation of the dynamics of charged particles in the influence of an electric field was validated by (Grosshans and Papalexandris, 2017c).

Specifically for the current set-up the implementation of the Eulerian solver for the fluid phase has been validated by Grosshans (2018) through comparison of the solution for a single-phase flow with the DNS data of Zhu et al. (2009) and Huser and Biringen (1993), which were also performed for a duct flow of $Re = 10\,000$. In general, for both average and fluctuating quantities of the gas flow a good agreement to the DNS data is ascertained.

In the present simulations an initially fully-developed turbulent flow field was considered. The particles were

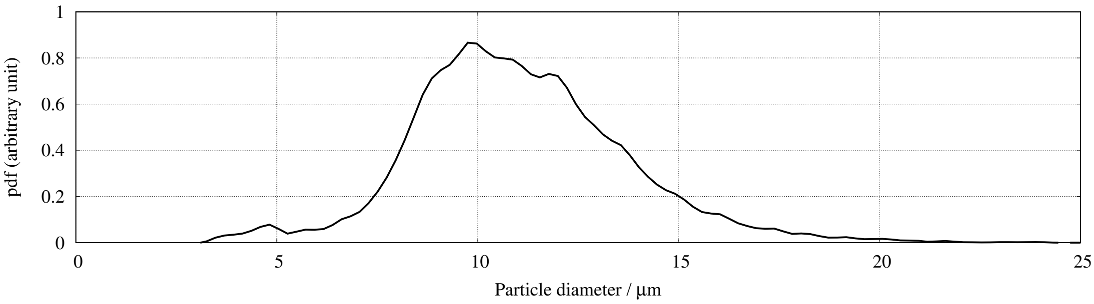

Figure 2: Experimental particle size distribution measured with a Coulter Counter, replicated in the simulations.

introduced at random positions whereas their initial velocity was assumed to equal the local velocity of the surrounding fluid. The particle size distribution, which is detailed in section 3.3, replicated the powder utilized in the experiments.

Since in the present study time-averaged data was analyzed, first the temporal convergence of the particle concentrations was evaluated. By monitoring the evolution of the normalized particle concentration in the viscous sublayer in a similar numerical set-up, Grosshans (2018) found that particle dispersion reached a statistically stationary state at about $t^+ = 40$. Considering a safety factor, in the present study we started to collect statistics from $t^+ = 90$ after particle injection. The statistics of the particle concentration converged after 30 time units, i.e. at $t^+ = 120$. Again, a safety factor was applied and statistics were collected between $t^+ = 90$ and $t^+ = 150$, which corresponds to about 70 flow-through times.

The particle solver was validated by Grosshans (2018) for the case of uncharged particles through comparison with the DNS data of Noorani et al. (2016). The flow Reynolds number was 11 386. Monodisperse particles were considered, and the solid mass loading ratio was 0.001. Given the dilute regime, Noorani et al. (2016) used a one-way coupled approach. Comparison of the particle concentrations in the viscous sublayer presented by Noorani et al. (2016) with data generated by our solver shows that the prediction of both the statistically stationary and instantaneous states are in good agreement.

3.3. Determination of the expected initial particle charge

The process of charge build-up is not included in the current simulations. Instead, the expected charge of the particles at the glass test section inlet is imposed as an initial condition in the simulations and varied systematically. By doing so, the effect of different levels electrostatic charge that the particles could acquire in the experimental apparatus is evaluated. For this purpose we first estimated the order of magnitude of the potential amount of charge carried by the particles when reaching the test section. This estimation serves as a basis for the decision on the parameter range to be investigated. With respect to the methodology for the evaluation, we compare the maximum charge predicted by the charging model implemented by Grosshans and Papalexandris (2017a) with the outcome of the charge relaxation model by Matsuyama (2018).

In the first approach, it is assumed that the charge originates from triboelectric effects during collisions of the particles with structural components such as the feeder or duct walls prior to the test section. While the amount of collisions taking place is unknown, one can utilize the dynamic model implemented by Grosshans and Papalexandris (2017a) to predict an order of magnitude of the maximum charge a particle can obtain. This charge value is also termed equilibrium charge, since for further collisions the amount of pre-charge transferred from the particle to the surface equals the triboelectric charge separation, i.e. the net charge transfer is zero. Following this model, even though the total equilibrium charge depends on the particle size, the equilibrium surface charge density, $q_{\rm eq}$ is independent. More precisely, for a theoretically infinite number of collisions the model predicts an asymptotic limit for q of

$$q_{\rm eq} = \frac{\varepsilon\, U}{h} \,. \qquad (9)$$

In this equation U denotes the contact potential and h the particle-surface separation distance. Consulting the well-known triboelectric series (e.g. Brück, 1981) one may assume a value of the order of 1 V for the contact potential. Concerning h, a commonly used es-

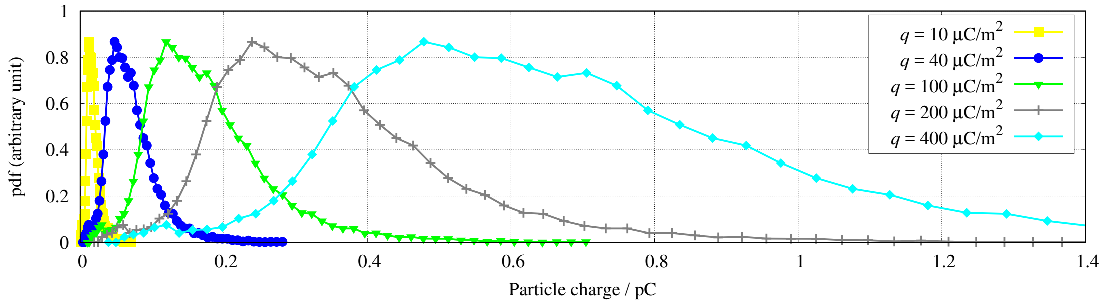

Figure 3: Charge distributions assigned to the particles in the simulations.

timate relates to the order of the range of repulsive molecular forces due to surface irregularities, namely $h = 10^{-9}$m (John et al., 1980; Kolniak and Kuczynski, 1989; Grosshans and Papalexandris, 2016b). These assumptions lead to a maximum charge density of $q_{\mathrm{eq}} = 8.85 \times 10^{-3}$ C/m^2.

However, as recently discussed by Matsuyama (2018), such a high value cannot be obtained in reality since a charge relaxation takes place immediately after the particle-surface contact. This relaxation occurs due to discharge at the contact gap when the potential difference equals the gaseous breakdown limit potential. Thus, this mechanism limits the maximum charge a particle can carry. Matsuyama (2018) compared in his work the prediction of the breakdown limit potential by Paschen's law with their impact charging experiments of single particles (cf. Matsuyama and Yamamoto, 1995, 1997; Matsuyama et al., 2003). The compared data set indicate that a particle of the size of 12 µm, which corresponds to the mean particle size in the present study, is able to carry a maximum charge of about 0.5 pC or, in other words, a surface charge density of about $q = 10$ µC/m^2.

For each of the simulations in this study, we assigned a charge density to the particles that remains constant as charge exchange is not considered. For comparison purposes one simulation was ran with an uncharged particulate phase. Other five cases with different charge density values, namely $q = 10$ µC/m^2, $q = 40$ µC/m^2, $q = 100$ µC/m^2, $q = 200$ µC/m^2, and $q = 400$ µC/m^2, were computed. In this way the parameter space explored uncharged particles, particles carrying a charge which corresponds to the limit predicted by the charge relaxation model, and up to 40 times the respective. This choice aims to give an overview of the effects of particle charge for conditions that are be expected in this type of flows. However, it is noted that there are several underlying assumptions which may not coincide with realistic conveying situations. These include the assumption of homogeneously distributed charge on the surface of each particle, which might not be reachable considering the finite number of collisions of the particle with the test rig. Also, the charge of the particulate phase might be dependent on the distance to the wall, i.e. a particle close to the wall is expected to accumulate more charge than a particle in the bulk of the flow. It is noted that the chosen charge levels do not aim to approximate a physically correct state, but rather to study the effect of homogeneous particle charge on the flow and particle dynamics.

A consequence of the decision to assign a constant surface charge density is the dependence of the total particle charge on its size. The experimental particle size distribution replicated in the simulations is plotted in figure 2. The resulting particle charge distributions when applying the surface charge densities in the simulations are given in figure 3.

4. Resulting particle concentrations

In the following, the experimental measurements are compared to the numerical results to evaluate the influence of electrostatic forces on the particle concentration profiles. The resulting mean concentration profiles along the laser sheet centerline normalized by the mean concentration at $y = 0.15\ H$ are plotted for the near-wall region in figure 4. Since the planar laser sheet was inclined by 18° with respect to the wall-normal (cf. figure 1) the z^+ position varies with the y^+ coordinate.

The differences in the numerical results reveal the potential influence of electrostatic charges on preferential particle concentration. The effect of the electrostatic charges on the particle concentrations is most pronounced in the vicinity of the wall, i.e. in the region

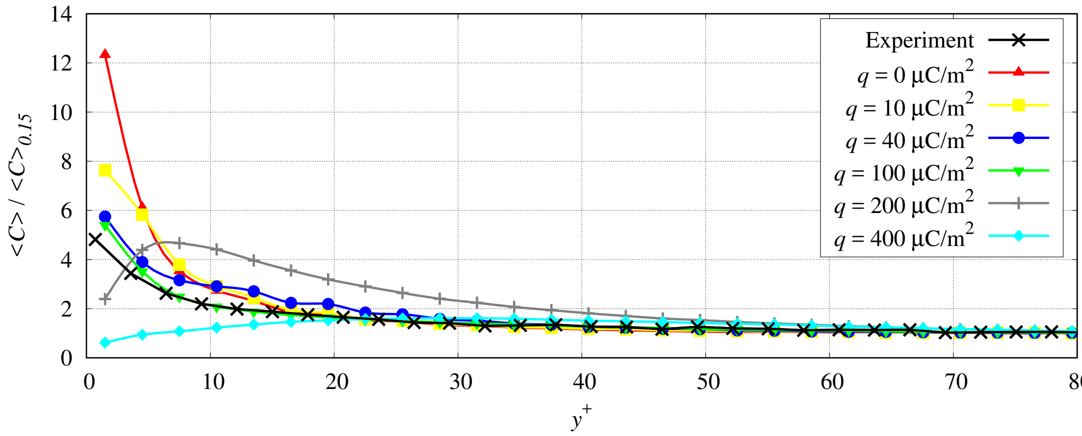

Figure 4: Comparison of the measured and simulated mean particle concentration distribution in the near-wall region. The local concentration is normalized by the mean concentration at $y = 0.15\ H$. Note that the plotted data is collected along the laser beam (cf. figure 1), i.e. the respective z^+ position varies with the y^+ coordinate.

$y^+ < 50$. Comparing the different numerical data suggests that the case corresponding to $q = 100\ \mu\mathrm{C/m}^2$ replicates the closest the experimental measurements, suggesting that the powder utilized in the experiments could be subjected to a charge of this order of magnitude. However, a full compliance between experiments and simulations cannot be expected from the present study. Discrepancies can be attributed to inaccuracies in the numerical methodology, namely the rather crude assumptions underlying the charge distribution discussed in the previous subsection. The boundary conditions to the electric field may also play a role: while in the simulations the wall is considered to be conductive and grounded, the corresponding components in the experimental facility consist of a mix of materials including grounded metal parts but also glass. On the other hand there are few differences in the data acquisition. In the numerical post-processing procedure all particles are counted whose center point resides within the thickness of the laser sheet. This means the detection of a parcel is independent of its size. There is no difference in the post-processing between parcels and particles besides the fact that a parcel represents several particles is taken into account.

However, the Gaussian intensity profile across the laser thickness in the experiments implies that there is a decrease of the probability to detect small particles at the beam flanks. The number of particles identified in the experimental images might also be affected by particle overlapping since the beam thickness is larger than the particle diameter.

All the profiles presented in figure 4 indicate the effect of turbophoresis, i.e. particle accumulation in the near-wall region. Comparing the uncharged numerical data with the charged cases shows that the peak at the wall reduces with increasing particle charge. This behavior was already observed by Grosshans (2018) and attributed to the increasing electrostatic forces between particles. These forces are most prominent in regions of high particle number density since the average spacing between particles is the lowest. Consequently, particles are pushed out of the near-wall region towards the bulk of the flow. In other words, electrostatic charges tend to smoothen the particle concentration profiles.

To get further insight, the mean particle concentrations over the complete duct cross-section are depicted in figure 5. The particle accumulation close to the walls can be observed for all cases. In particular, the distributions relating to the uncharged particles (figure 5(a)) exhibit the strongest peaks at the four corners of the duct. Additional maxima are formed at the centerlines of the four sidewalls. These characteristic peaks in the ducts corner and sidewalls centerlines are in qualitative agreement with the observations of Noorani et al. (2016) and Tabaei Kazerooni et al. (2017).

When a charge is assigned (figures 5(b)–5(f)) the particles are forced to migrate from the regions with the highest accumulation, i.e. the duct corners and the walls' bisector. Nevertheless, for the smallest charge density of $q = 10\ \mu\mathrm{C/m}^2$ (figure 5(b)) the particles, instead of migrating to the bulk of the flow, they travel along the sidewalls. Especially the peaks at the

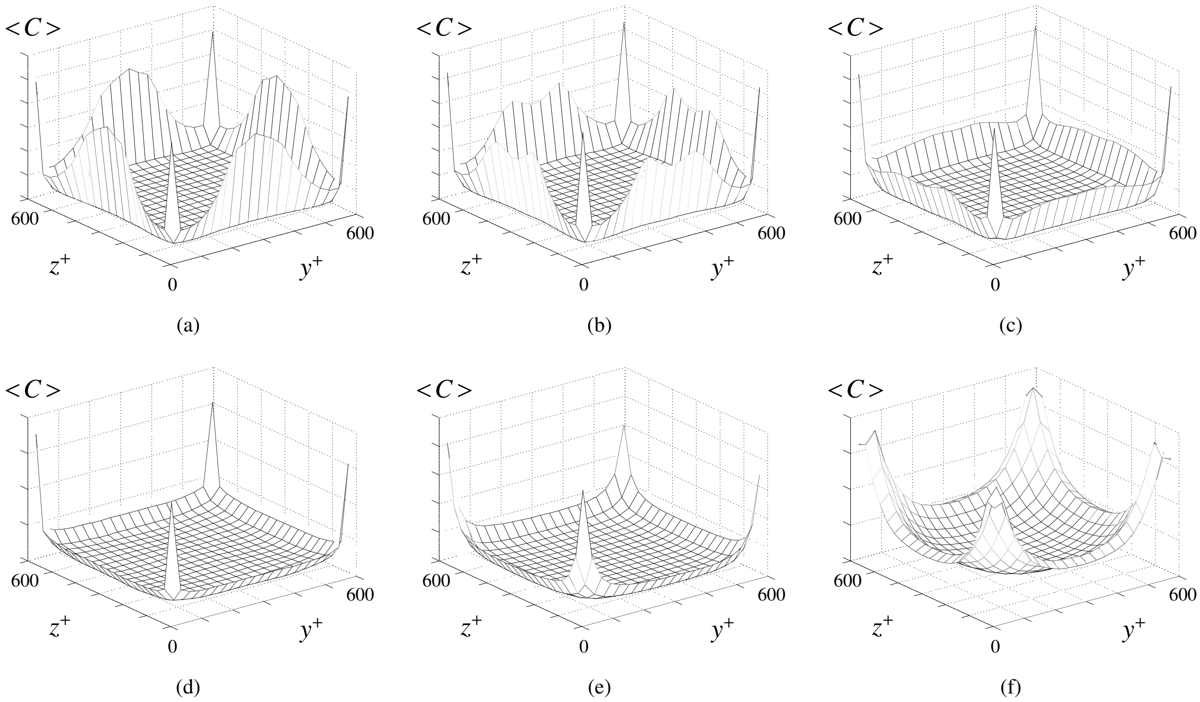

Figure 5: Mean particle concentration in arbitrary units, $< C >$, over the duct cross-section. The particles carry a surface charge density q of (a) 0 μC/m^2, (b) 10 μC/m^2, (c) 40 μC/m^2, (d) 100 μC/m^2, (e) 200 μC/m^2 and (f) 400 μC/m^2. Note that $< C >$ is normalized by the maximum local concentration of each case, i.e. the vertical axes of the figures are scaled differently.

walls' bisector are efficiently reduced through the arising forces which lead to a more smooth particle concentration at the walls. If the charge density is increased to q = 40 μC/m^2 (figure 5(c)), the forces between the particles residing in the high number-density regions become even higher and, thus, the peaks are further smoothed out. While the particles still accumulate at the corners and at the walls, only slight peaks at the walls' bisector remain. For a further increase to q = 100 μC/m^2 (figure 5(d)) these peaks finally vanish completely. Also, for this charge density the inter-particle forces become sufficiently high so that the particles residing in the duct corners may overcome their inertial migration induced by secondary flows. Consequently, the number-density in these regions is efficiently reduced. This effect remains qualitatively similar when a charge density of q = 200 μC/m^2 (figure 5(e)) and q = 400 μC/m^2 (figure 5(f)) is assigned, but the electrostatic forces affect an even stronger smoothing of the concentrations. Therefore, the peaks at the corners are further reduced and particles migrate along the walls and towards the bulk of the flow. Keeping in mind the location of the laser beam (cf. figure 1), the observed mechanism related to inter-particle electrostatic forces reduces the maxima of the related profiles in figure 4. Finally, for the case of q = 400 μC/m^2 only slight particle accumulation in the near-wall region is detectable.

Another interesting behavior is that the peaks detected in the simulations detach from the wall for a certain charge density. For q = 200 μC/m^2 the peak shifts to $y^+ \approx 8$ and for q = 400 μC/m^2 to $y^+ \approx 40$. Note that the former peak shift is not detectable in figure 5(e) since this spatial shift is below the width of the chosen bins. This migration may be related to the residence of particles at the duct walls which are supported by induced image charges. Rather high charge is accumulated in these residence regions which pushes the remaining airborne particles towards the bulk of the flow.

5. Conclusions

We examined the role of accidentally accumulated electrostatic charge in the mean particle concentration distribution for a realistic test case, and in particular the near-wall region where turbophoresis is responsible for increased concentrations.

Numerical simulations of particles of equal polarity in a fully developed duct flow were performed considering a homogeneous charge density on the particles' surface. Whereas the simulations reproduced the particle size distribution measured in the experiments the charge density was varied systematically. The resulting concentration profiles were compared to experimental data for which the particle charge is unknown. The numerical parametric study reveals that electrostatic charges play an important role in the particle redistribution, especially in the near-wall region. In general, the simulations corroborate that the electrical forces tend to smoothen the particle concentration profiles, i.e. counteract particle accumulation through turbophoresis. The numerical results for a surface charge density of 100 $\mu C/m^2$ are the closest to the experimental data.

A future elaboration of this topic requires the simulation of the charge build-up process in order to get a more realistic picture of the charge distribution of the powder, as well as the detailed analysis of the formation and the effect of deposition layers at the duct walls. The present study focused on dilute suspensions and did not attempt to capture the formation of deposition layers. In this context the mathematical framework utilized the assumption of unity gas volume fraction and neglected van der Waals forces and particle polarization.

6. Acknowledgments

The authors gratefully acknowledge the financial support from the Max Buchner Research Foundation (HG), the Advanced Simulation and Computing program of the US Department of Energys National Nuclear Security Administration via the PSAAP-II Center at Stanford, Grant No. DE-NA0002373-1 (LV and AB) and the National Research Fund of Belgium (FNRS) under the GRANMIX Projet de Recherche grant (MP).

References

Adhiwidjaja, I., Matsusaka, S., Yabe, S., Masuda, H., 2000. Simultaneous phenomenon of particle deposition and reentrainment in charged aerosol flow – effects of particle charge and external electric field on the deposition layer. Adv. Powder Technol. 11 (2), 221–233.

Boris, J. P., Grinstein, F. F., Oran, E. S., Kolbe, R. L., 1992. New insights into large eddy simulation. Fluid Dyn. Res. 10, 199–228.

Bracco, F. V., 1985. Modeling of engine sprays. SAE Tech. Pap. 850394.

Brück, R., 1981. Chemische Konstitution und elektrostatische Eigenschaften von Polymeren. Kunststoffe 71, 308–312.

Eaton, J. K., Fessler, J. R., 1994. Preferential concentration of particles by turbulence. Int. J. Multiphase Flows 20, 169–209.

Egan, S., 2017. Learning lessons from five electrostatic incidents. J. Electrostatics 88, 183–189.

Elgobashi, S., 1994. On predicting particle-laden turbulent flows. Appl. Sci. Res. 52, 309–329.

Fath, W., Blum, C., Glor, M., Walther, C.-D., 2013. Electrostatic ignition hazards due to pneumatic transport of flammable powders through insulating or dissipative tubes and hoses – new experiments and calculations. J. Electrostat. 71 (3), 377–382.

Glor, M., 2003. Ignition hazard due to static electricity in particulate processes. Powder Technol. 135–136, 223–233.

Grossel, S. S., 2012. Design and operating practices for safe conveying of particulate solids. J. Loss Prev. Process Ind. 25, 848–852.

Grosshans, H., 2018. Modulation of particle dynamics in dilute duct flows by electrostatic charges. Phys. Fluids 30 (8), 083303.

Grosshans, H., Papalexandris, M. V., 2016a. Evaluation of the parameters influencing electrostatic charging of powder in a pipe flow. J. Loss Prev. Process Ind. 43, 83–91.

Grosshans, H., Papalexandris, M. V., 2016b. Large eddy simulation of triboelectric charging in pneumatic powder transport. Powder Technol. 301, 1008–1015.

Grosshans, H., Papalexandris, M. V., 2016c. A model for the non-uniform contact charging of particles. Powder Technol. 305, 518–527.

Grosshans, H., Papalexandris, M. V., 2017a. Direct numerical simulation of triboelectric charging in a particle-laden turbulent channel flow. J. Fluid Mech. 818, 465–491.

Grosshans, H., Papalexandris, M. V., 2017b. Numerical study of the influence of the powder and pipe properties on electrical charging during pneumatic conveying. Powder Technol. 315, 227–235.

Grosshans, H., Papalexandris, M. V., 2017c. On the accuracy of the numerical computation of the electrostatic forces between charged particles. Powder Technol. 322, 185–194.

Grosshans, H., Villafañe, L., Banko, A., Papalexandris, M. V., April 2018. Influence of electrostatic charges on the particle concentration in wall-bounded turbulent flows. In: 8th World Congress on Particle Technology. Orlando, FL, USA.

Guardiola, J., Rojo, V., Ramos, G., 1996. Influence of particle size, fluidization velocity and relative humidity on fluidized bed electrostatics. J. Electrostat. 37 (1–2), 1–20.

Gullbrand, J., Bai, X. S., Fuchs, L., 2001. High-order Cartesian grid method for calculation of incompressible turbulent flows. Int. J. Num. Meth. Fluids 36, 687–709.

Hendrickson, G., 2006. The novelty of the presented formulation lies in the inclusion of electrostatic forces in the stochastic formulation as outlined below. Chem. Eng. Sci. 61, 1041–1064.

Hogue, M., Calle, C. I., Weitzman, P. S., Curry, D. R., 2008. Calculating the trajectories of triboelectrically charged particles using discrete element modeling (dem). J. Electrostat. 66, 32–38.

Huser, A., Biringen, S., January 1993. Direct numerical simulation of turbulent flow in a square duct. In: 31st Aerospace Sciences Meeting & Exhibit. Reno, NV.

Jang, G. S., Shu, C. W., 1996. Efficient implementation of weighted ENO schemes. J. Comput. Phys. 126, 202–228.

John, W., Reischl, G., Devor, W., 1980. Charge transfer to metal surfaces from bouncing aerosol particles. J. Aerosol Sci. 11 (2), 115–138.

Kallio, G. A., Reeks, M. W., 1989. A numerical simulation of particle deposition in turbulent boundary layers. Int. J. Multiphase Flows 15, 433–446.

Kolehmainen, J., Ozel, A., Sundaresan, S., 2018. Eulerian modelling of gas–solid flows with triboelectric charging. J. Fluid Mech. 848, 340–369.

Kolniak, P. Z., Kuczynski, R., 1989. Numerical modeling of powder electrification in pneumatic transport. J. Electrostat. 23, 421–430.

Kuerten, J. G. M., van der Geld, C. W. M., Geurts, B. J., 2011. Turbulence modification and heat transfer enhancement by inertial particles in turbulent channel flow. Phys. Fluids 23 (12), 123301.

Lenert, A., Wang, E. N., 2012. Optimization of nanofluid volumetric receivers for solar thermal energy conversion. Sol. Energy 86 (1), 253 – 265.

Lim, E. W. C., Yao, J., Zhao, Y., 2012. Pneumatic transport of granular materials with electrostatic effects. AIChE J. 58 (4), 1040–1059.

Marchioli, C., Soldati, A., 2002. Mechanisms for particle transfer and segregation in a turbulent boundary layer. J. Fluid Mech. 468, 283–315.

Matsuyama, T., 2018. A discussion on maximum charge held by a single particle due to gas discharge limitation. In: AIP Conference Proceedings. Vol. 1927. American Institute of Physics, p. 02001.

Matsuyama, T., Ogu, M., Yamamoto, H., Marijnissen, J. C. M., Scarlett, B., 2003. Impact charging experiments with single particles of hundred micrometre size. Powder Technol. 135–136, 14–22.

Matsuyama, T., Yamamoto, H., 1995. Charge relaxation process dominates contact charging of a particle in atmospheric conditions. J. Phys. D: Appl. Phys. 28, 2418–2423.

Matsuyama, T., Yamamoto, H., 1997. Charge relaxation process dominates contact charging of a particle in atmospheric conditions: II. The general model. J. Phys. D: Appl. Phys. 30, 2170–22175.

McLaughlin, J. B., 1989. Aerosol particle deposition in numerically simulated channel flow. Phys. Fluids 1, 1211–1224.

Moore, A. D. (Ed.), 1973. Electrostatics and its Applications. Wiley, New York, NY, US.

Noorani, A., Vinuesa, R., Brandt, L., Schlatter, P., 2016. Aspect ratio effect on particle transport in turbulent duct flows. Phys. Fluids 28 (11), 115103.

Ray, M., Chowdhury, F., Sowinski, A., Mehrani, P., Passalacqua, A., 2018. An Euler-Euler model for mono-dispersed gas-particle flows incorporating electrostatic charging due to particle-wall and particle-particle collisions. Chem. Eng. Sci.

Schiller, L., Naumann, A. Z., 1933. A drag coefficient correlation. Z. Ver. Dtsch. Ing. 77, 318–320.

Schwindt, N., von Pidoll, U., Markus, D., Klausmeyer, U., Papalexandris, M. V., Grosshans, H., 2017. Measurement of electrostatic charging during pneumatic conveying of powders. J. Loss Prev. Process Ind. 49, 461–471.

Sippola, P., Kolehmainen, J., Ozel, A., Liu, X., Saarenrinna, P., Sundaresan, S., 2018. Experimental and numerical study of wall layer development in a tribocharged fluidized bed. J. Fluid Mech. 849, 860–884.

Song, D., Mehrani, P., 2017. Mechanism of particle build-up on gas-solid fluidization column wall due to electrostatic charge generation. Powder Technol. 316, 166–170.

Soo, S. L., 1971. Dynamics of charged suspensions. In: Topics in Current Aerosol Research. Pergamon Press, pp. 71–73.

Stiesch, G., 2003. Modeling Engine Spray and Combustion Processes. Springer Verlag, Berlin Heidelberg New York.

Sumer, B. M., Deigaard, R., 1981. Particle motions near the bottom in turbulent flow in an open channel. Part 2. J. Fluid Mech. 109, 311–337.

Tabaei Kazerooni, H., Fornari, W., Hussong, J., Brandt, L., 2017. Inertial migration in dilute and semidilute suspensions of rigid particles in laminar square duct flow. Phys. Rev. Fluids 2, 1–23.

Tanoue, K., Ema, A., Masuda, H., 1999. Effect of material transfer and work hardening of metal surface on the current generated by impact of particle. J. Chem. Eng. Jpn. 32, 544–548.

Tanoue, K., Tanaka, H., Kitano, H., Masuda, H., 2001. Numerical simulation of tribo-electrification of particles in a gas-solid two-phase flow. Powder Technol. 118, 121–129.

Tsuji, Y., Morikawa, Y., 1982. LDV measurements of an air-solid two-phase flow in a horizontal pipe. J. Fluid Mech. 120, 385–409.

Tsuji, Y., Morikawa, Y., Shiomi, H., 1984. LDV measurements of an air-solid two-phase flow in a vertical pipe. J. Fluid Mech. 139, 417–434.

Villafañe, L., Banko, A., Elkins, C., Eaton, J. K., 2017. Gas heating by radiation absorbing inertial particles in a turbulent duct flow. In: Annual Research Briefs. Center for Turbulence Research, Stanford University, USA.

Watano, S., Saito, S., Suzuki, T., 2003. Numerical simulation of electrostatic charge in powder pneumatic conveying process. Powder Technol. 135–136, 112–117.

Zhu, Z., Yang, H., Chen, T., 2009. Direct numerical simulation of turbulent flow in a straight square duct at Reynolds number 600. J. Hydrodyn. 21, 600–607.